

Elementary Implementation of VTK XML files

A FEMDEM Application

JOHN-PAUL LATHAM^{*†}, ADO FARSI^{*†}, and MICHAEL TRAPP^{*}

A recent state-of the arts review by EU decision makers [1] revealed that current building guidelines are not taking into account threats such as natural disasters and acts of terrorism. Updating these guidelines requires accurate numerical models to quantify the resilience of building elements against explosive and projectile impact.

The Applied Modelling and Computation Group (AMCG) at Imperial College London has recently developed a novel coupled dynamic gas/solid FEMDEM code.

In this paper, this Y code is applied to simulate 2D projectile impact on laminated glass. Furthermore, a novel implementation is presented to prepare and write VTK output files. Before, obsolete external VTK libraries were required to visualise the code output.

The simulation results are not realistic, indicating errors in the preparation software or in the underlying code. The implementation of VTK files is successful and valid output files are produced. The files are visualisable using Paraview.

CCS Concepts: • **Applied computing** → *Engineering*.

^{*}Imperial College London.

[†]Supervisor

Authors' address: John-Paul Latham, j.p.latham@imperial.ac.uk; Ado Farsi, ado.farsi@imperial.ac.uk; Michael Trapp, mt5918@ic.ac.uk.

Permission to make digital or hard copies of all or part of this work for personal or classroom use is granted without fee provided that copies are not made or distributed for profit or commercial advantage and that copies bear this notice and the full citation on the first page. Copyrights for components of this work owned by others than ACM must be honored. Abstracting with credit is permitted. To copy otherwise, or republish, to post on servers or to redistribute to lists, requires prior specific permission and/or a fee. Request permissions from permissions@acm.org.

© 2019 Association for Computing Machinery.

XXXX-XXXX/2019/1-ART1 \$15.00

<https://doi.org/123456789>

Additional Key Words and Phrases: FEMDEM, VTK, Legacy, XML, base64, encoding

ACM Reference Format:

John-Paul Latham, Ado Farsi, and Michael Trapp. 2019. Elementary Implementation of VTK XML files: A FEMDEM Application. *ACM Trans. Model. Comput. Simul.* 1, 1, Article 1 (January 2019), 25 pages. <https://doi.org/123456789>

1 PHYSICS THEORY

1.1 Laminated Glass Model

Laminated glass is a sandwich structure of two brittle glass plies and an adhered polymer inter-layer (or inter-face) in between. The bonding between the glass and the inter-layer is without physical adhesive [2]. Secondary laminated glass consists of two such laminates, separated by a layer of air.

Advantageous properties of laminated glass include a relatively high penetration resistance [3], low weight [4] and the adherence of fractured glass fragments to the structure to reduce the risk of injuries [3, 5, 6, 7]. Breakage of the inner ply significantly reduces strength and facilitates a full collapse of the glass [6]. An optional back layer (usually poly-carbonate (PC) [8, 9]) improves structural stability and additional energy absorption [8, 10].

The prediction of crack initiation and propagation poses a significant challenge and requires ongoing research effort. Local stress intensification is caused by pre-existing micro-structural material flaws¹ such as micro-cracks and voids [11].

¹inhomogeneities, discontinuities

Many fracture models have been proposed. The Y code uses a local combined single and smeared crack model approach [12, 13], in which a single crack is replaced by a blunt crack band [14].

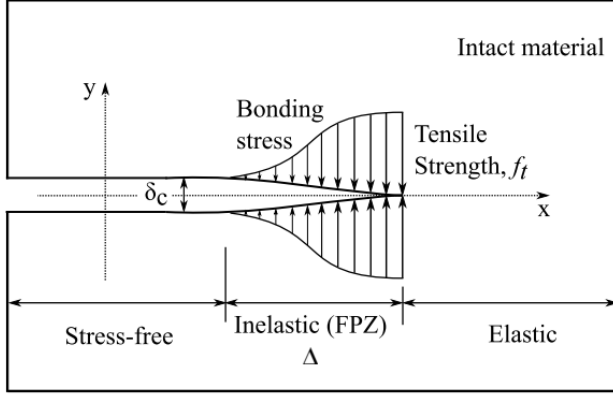


Fig. 1. Single Crack (Dugdale) Model. [15]

The single crack model in Fig. 1 assumes a crack tip located in a fracture process zone (FPZ). Plastic bonding stress $\sigma \leq f_t$ causes the crack tip to open up, up to a critical separation length $\delta = \delta_c$ [15].

To determine the bonding stress, the Y code adopts the Mohr-Coulomb constitutive model [13], described by

$$\tau = c + \sigma \tan \phi, \quad (1)$$

with shear stress τ , normal stress σ , internal cohesion c and internal friction angle ϕ . The internal friction coefficient is given by

$$\eta = \tan \phi \quad (2)$$

The stresses σ and τ correspond to normal and shear displacements δ_n and δ_s and tensile and shear strengths f_t and f_s . These material strengths are defined as the maximum strength in the stress-displacement diagram (Fig. 2), with maximum elastic displacement δ_p and critical displacement δ_s .

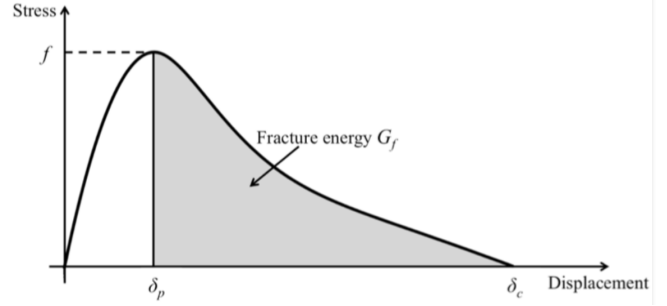


Fig. 2. Stress-displacement curve according to the single and smeared crack model. [13]

The fracturing in the strain-softening part is modelled using joint elements which are generated between two neighbouring shell elements. Cracks coincide with the element edges [15].

Further description is given by Latham et al [13], Munjiza et al [14], Lei et al [16] and Chen and Chang [17].

1.2 Inter-layer Model

The task of the inter-layer is the absorption of impact energy and the maintenance of adhesion to the plies [4]. The inter-layer consists of one or more sheets. Common inter-layer materials include polymers such as polyvinyl butyral (PVB), thermoplastic polyurethane (TPU), and most recently SentryGlas®Plus (SGP) [18, 19].

Mechanical properties of the inter-layer are dependent on the fracture state of the laminated glass [20]. Prior to fracture, straining of the inter-layer is limited, permitting the application of linear visco-elastic laws. After the failure of the glass, the inter-layer is subject to large strains and linear visco-elasticity is no longer applicable. Instead, the inter-layer is modelled as a hyper-elastic material [21, 22]. Work done by stresses onto such materials only depends on the reference state X and the current state x , but not on the load path (Fig. 3). Deformation from X to x is described by a deformation gradient [23]

$$F = \frac{d\varphi}{dX} \quad (3)$$

with mapping function φ mapping from X to x .

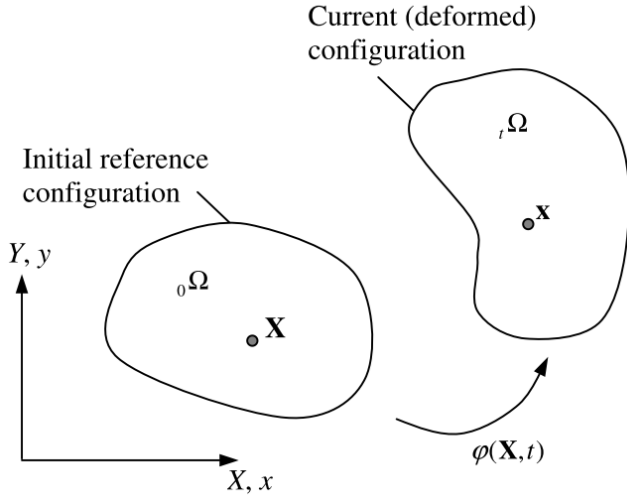


Fig. 3. Deformation from reference to current state. [23]

Hyper-elastics are mathematically described by a characteristic strain energy density function W . One of the simplest hyper-elastic models is the Neo-Hookean model [21] whose characteristic function is given by

$$W = \frac{\mu_0}{2} (I_1 - 3) - \mu_0 \ln J + \frac{\lambda_0}{2} \ln^2 J, \quad (4)$$

with Lamé constants λ_0 and μ_0 from the linearised theory, $J = |F|$ and first invariant $I_1 = C_{II}$ with right Cauchy stress tensor [21]

$$C_{ij} = F_{ii} F_{jj}. \quad (5)$$

Upper case indices refer to the reference configuration, while lower case indices refer to the current configuration.

Another common, simple hyper-elastic model is the Mooney - Rivlin model [24, 25]. The characteristic strain energy function for the compressible 2-Parameter Mooney - Rivlin model [25] is given by

$$W_2 = C_{10} (\bar{I}_1 - 1) + C_{01} (\bar{I}_2 - 1) + \frac{1}{d} (J - 1), \quad (6)$$

where C_{10} and C_{01} are adjustable parameters, $d = 2 / K$ with bulk modulus K and $\bar{I}_1 = J^{-\frac{1}{3}} I_1$ and $\bar{I}_2 = J^{-\frac{1}{3}} I_2$ are deviatoric invariants [24]. The second invariant is given by

$$I_2 = \frac{1}{2} (C_{JJ}^2 - C_{IK} C_{KI}). \quad (7)$$

Other hyper-elastic models [24] include a more general polynomial model, Arruda-Boyce, Ogden and Yeoh. For the polynomial model, customized coefficients [2] already exist in the literature, specifically for laminated glass.

Modelling the occurrence of fracture needs to be permitted for the inter-layer as well, as fracturing of the inter-layer is possible. This consideration necessitates the extension of the smeared single and combined fracture model to the inter-layer.

2 NUMERICAL MODELLING THEORY

2.1 FEMDEM Model

The combined finite-discrete element method, FEMDEM or FDEM [3, 12, 14, 17, 19, 26, 27, 28, 29, 30], contains discrete element that interact with neighbouring discrete elements. In addition, each discrete element is discretised into finite elements. Each finite element mesh captures the deformability of a discrete element.

Fracture and fragmentation is modelled as a transition from continua to discontinua. It is also in principle possible to imagine an inverse process of particles merging together. [14]

Based on the 3D FDEM code Y3D by Munjiza et al [12, 14, 26], Xiang et al [31] added many detailed improvements and features to the code. The new model, Solidity, is capable of creating realistic coupled multi-physics simulations. In contrast to

conventional models, Solidity is not reliant on element deformability restriction constraints (due to the locking problem) and uses simpler triangular, quadratic and tetrahedral elements [13].

2.2 Governing Equations

The governing equations for the finite element calculations in the FEMDEM method are the equations of motion. The equations are given by

$$M\ddot{x} + \mu\dot{x} + f_{\text{int}} = f_{\text{ext}} = f_l + f_b + f_c, \quad (8)$$

with lumped nodal mass matrix M , nodal displacements x , viscosity μ , internal nodal forces f_{int} and external nodal forces f_{ext} . External forces consist of external loads f_l , bonding forces f_b and contact forces f_c . Internal forces f_{int} are generated by element deformation. FEMDEM systems solve these equations via explicit time integration using the forward Euler method [16].

2.3 Contact Detection

The combination of discrete and finite elements is established via an interaction algorithm [16]. This algorithm consists of contact detection [32] and contact interaction [28]. Contact detection is carried out using search algorithms.

The contact detection algorithm detects couples of discrete elements close to each other by eliminating couples of discrete elements that are too far from each other to be in contact. In other words, contact detection avoids processing contact interaction when there is no contact. This reduces CPU requirements and processing run time [14].

Contact interaction is only considered for discrete elements which are within a buffer size b of each other, given by

$$b = 0.1 \Delta_{\min}, \quad (9)$$

where Δ_{\min} is the minimum edge².

²minimum element side length, minimum size

2.4 Contact Interaction

Penetration of a contractor³ body into a target⁴ body is implemented in the Y code by the potential contact force method, see Fig. 4 [14]. Assumption of a conservative force field enables a description of the contact forces using potentials,

$$f_c^{2D} = -f_t^{2D} = \oint_{\Gamma_{\beta_t \cap \beta_c}} n_{\Gamma} (\varphi_c - \varphi_t) d\Gamma, \quad (10)$$

$$f_c^{3D} = -f_t^{3D} = \int_{S_{\beta_t \cap \beta_c}} n_S (\varphi_c - \varphi_t) dS, \quad (11)$$

with force potentials φ and outward unit normal n to the penetration boundary Γ or surface area S .

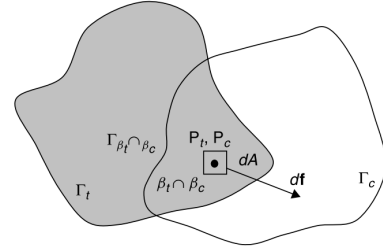


Fig. 4. Infinitesimal overlap of contractor and target body. [14]

The penetration distance d for each case is given by [14]

$$d = \frac{\sigma h}{p}, \quad (12)$$

with applied pressure σ , element height h and penalty factor p .

The penalty factor p is given by

$$p = \alpha E, \quad (13)$$

with Young's Modulus E and a constant α (in this paper: $\alpha = 10$) to regulate penetration.

³index c

⁴index t

Contact damping⁵ due to plastic deformation, breakage of surface asperities, etc. is given by [14]

$$\sigma_C = 4\xi \frac{\sqrt{p/\rho}}{h} \dot{d}, \quad (14)$$

with damping ratio $0 \leq \xi^6 \leq 1$ and finite element density ρ .

The mass damping coefficient is given by

$$\zeta = \sqrt{E\rho} \quad (15)$$

3 NUMERICAL MODEL APPROACH

3.1 Workflow

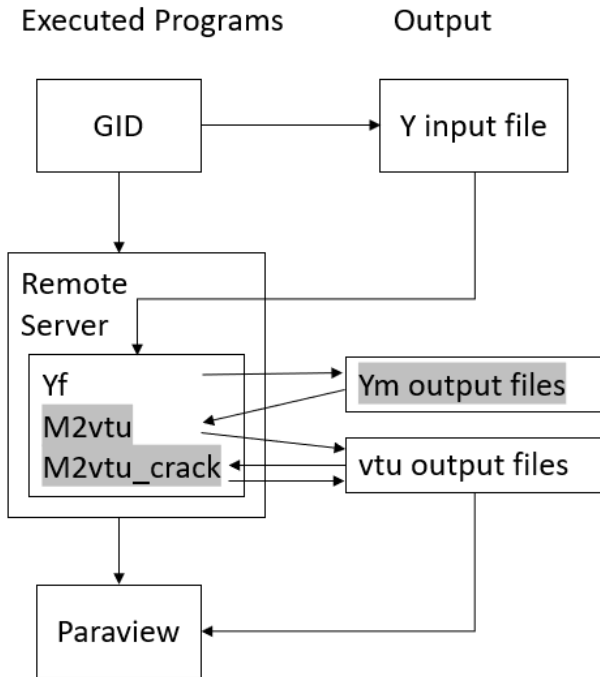


Fig. 5. Workflow of generating a simulation

The conducted workflow to generate simulations is illustrated in Fig. 5. The grey shaded items are

⁵Rayleigh damping, viscous damping

⁶describes energy dissipation

ready to be removed using the results from this paper such that the Yf code generates the VTK output files directly.

The required operating system presumably is Ubuntu 14.4, although this could not be confirmed using Travis CI automatic testing (url: <https://travis-ci.org/>). Therefore, the exact requirements are not known to the author at this point. The workflow was tested on Ubuntu 18.04.2 LTS subsystem for windows 10.

An input Y file is generated using the open source pre-processor CAD software GID [33] on Windows 10. It is possible to instead import the geometry from other CAD software, such as AutoCAD, although this approach is suspected to potentially cause errors.

With the input Y file as an argument, the program is compiled using three binary executables Yf, m2vtk and m2vtk_crack. The executables are generated using a make file, along with the Y2D code files, written in the programming language C. The code may be obtained from the AMCG at Imperial College London.

Code execution requires obsolete VTK 5.8 libraries. Tests to produce simulations were thus conducted exclusively on the high performance computing (HPC) system at Imperial College. Another private remote server was available for testing, but could not be employed due to extremely high latency.

The code outputs .vtu files which are combined to a time series simulation. The output is visualised using the open source software Paraview (url: <https://www.paraview.org/>).

3.2 Geometry Setup

The input Y file contains the model including geometry, constraints, materials and simulation parameters. The majority of modelling parameters are added from the literature. A list of material

parameters is given in Table 1. A list of input file simulation parameters is provided in Table 2. Auxiliary parameters are provided in Table 3.



Fig. 6. 2D geometry of the laminated glass structure and projectile [17]

Fig. 6 illustrates the 2D geometric setup. The figure shows the initial state of the projectile (yellow) immediately before impact on the laminated glass (impactor glass plies in red, inner glass ply in blue, inter-layer in green). The glass is fixed via a support system (in brown). The undersurface (the bottom lines) of the support structure contains no-velocity boundary conditions.

The dimensions are given in Fig. 7. The mesh for all bodies consists of triangular elements. The element size is 1 mm.

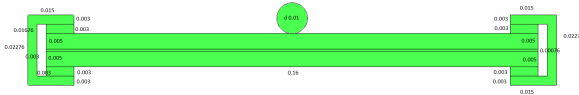


Fig. 7. Dimensions of the test geometry

3.3 Material Parameters

Table 1 lists the material parameters for glass, PVB, steel and rock. The literature provides values for most quantities, although values vary to a great extent in some cases. The values used in this paper are marked bold.

3.4 Problem Parameters

⁷for reference

⁸Rayleigh damping, viscous damping

⁹not relevant for glass, PVB and steel

¹⁰at laboratory conditions

The radius of the steel circle is set to 2.5 mm. The critical time step [41]¹¹ is set accordingly to

$$\Delta t_{\text{crit}} = \sqrt{\frac{V_e^{12} \rho^{13}}{p}} = \sqrt{\frac{0.000413 \cdot 7.8 \cdot 10^3}{4 \cdot 10^{11}}} \text{ s}. \quad (16)$$

The acceptable time step Δt is given by

$$\Delta t = \lfloor \Delta t_{\text{crit}} \rfloor = 3e - 6 \text{ s}, \quad (17)$$

where $\lfloor \cdot \rfloor$ denotes the floor operator. To simulate real time $t = 10 \text{ s}$, the maximum number of time steps required [41]¹¹ is given by

$$n_t = \frac{t}{\Delta t} = \frac{10 \text{ s}}{3e - 6 \text{ s}} = 1e6. \quad (18)$$

3.5 Verification

Meeting specified accuracy standards [1] requires verification of the numerical model by use of data from previous numerical experiments.

Physical experiments involving the breakage of glass require special safety arrangements. Impact experiments are being conducted outdoors by service company Jabisupra [42] in cooperation with Imperial College London. The company is active in the field of envelope security and specialises in protecting infrastructure from certain threats. Data for from this company was not ready and could not be used for this project.

Many other researchers have already conducted impact experiments in the past. A majority of the findings from these experiments are applicable to verify the model for this project.

¹¹ for inquiries concerning this reference please contact the AMCG at Imperial College London

¹²volume (in m^3) of the smallest finite element, without units

¹³density (in kg/m^3) of the material of the smallest finite element, without units

Table 1. List of Y2 input material parameter values.

Property	Glass	PVB	Steel Projectile	Rock ⁷
Density ρ [kg/m ³]	2500 [17, 24, 30, 34, 35]	870 [30] 1100 [17, 34, 35] 1105e3 [17]	7800 [17]	2700
Young's Modulus E [Pa]	7e10 [17, 34, 35] 7.409e10 [30] 7.41e10 [17] 7.5e10 [24]	1e8 [17] 2.2e2 [35] 5e10 [30]	2e11 [17]	3e10
Poisson's Ratio ν	0.2 [17, 30] 0.21 [24] 0.3 [17] 0.22 [34] 0.23 [35] 0.25 [17]	0.42 [17] 0.45 [24] 0.48 [30] 0.49 [32] 0.495 [35]	0.29 [17]	0.205
Mass damping coefficient μ^8 (see Eq. 15)	1.32e7	3.31e5	1.25e8	2.85e7
Elastic penalty term (see Eq. 13)	7e11	1e9	2.0e12	3.0e11
Contact penalty (see Eq. 13)	7e11	1e9	2.0e12	3.0e11
Mode I energy rate G_I [J/m ²]	10 [34] 3.9 [17] 4.0 [17]	2.8e3 [36] 20 [17]	1.9e5 [37]	20.0
Mode II energy rate G_{II} [J/m ²]	50 [34]	2.8e3	1.9e5	100.0
Mode III energy rate G_{III} [J/m ²]	50 [34]	2.8e3	1.9e5	100.0
Tensile Strength σ [Pa]	6e7 [32] 3e7 [17] 3.46e7 [17]	2e7 [38] 1.862e7 [17]	1e7 [4]	4e6
Shear Strength τ [Pa]	17.9 [17]	17.9 [17]		
Internal friction coefficient η (Eq. 2)	0.1 [32]	0.7 [20]	0.15 [39]	0.6
Internal cohesion c [Pa] (Eq. 1)	7e10	2.2e2	2e11	8e6
Pore fluid pressure ⁹ [Pa]	0	0	0	0
Joint friction coefficient ⁹	0.6	0.6	0.6	0.6
Joint roughness coefficient JRC_0 ^{9, 10}	15	15	15	15
Joint compressive strength JCS_0 ^{9, 10} [MPa]	120	120	120	120
Joint sample size [m] ⁹	0.2	0.2	0.2	0.2
Interface friction	0.1 [32]	0.62 [40]	0.44 [40]	0.6
2D Problems	plane strain			

Table 2. List of Y2D input simulation parameter values.

Parameter	Value
Maximum number of timesteps n_t (Eq. 18)	2e6
Current number of timesteps	0
Restart file saving frequency	1e2
Gravity in X Direction (m/s ²)	0
Gravity in Y Direction (m/s ²)	0
Gravity in Z Direction (m/s ²)	-9.8
Timestep (s) (Eq. 17)	1e - 6
Output frequency	2e3
Current number of iterations	0
Gravity setting stage (s)	0
Load ramping stage (s)	0
Maximum dimension (m)	10
Maximum force (N)	1e6
Maximum velocity (m/s)	100
Maximum stress (Pa)	1e8
Maximum displacement (m)	0.1
Minimum joint aperture (m)	1e - 7
Maximum contacting couples	1e7
Buffer Size b for NBS (m) (Eq. 9)	7.60e - 5
Accuracy (bit)	32
Joint friction model	Coulomb
Initial aperture correlation	roughness

Dynamic impact on laminated glass comprises hard and soft body impact [43]. Hard body impact such as ballistic impact [8] causes minimal deformation to the projectile, while soft body impact such as bird impact [43] causes the projectile to undergo extensive deformation.

Relevant parameters of the impact projectile include the normal velocity [4, 44, 45, 46], the mass [45, 46], the angle [44, 45, 46], the shape [46] and the size [4]. Relevant parameters for the outer glass ply include its dimensions [19], its mass, the support conditions [19] and the make-up [19]. For the inter-layer, the material [9, 18, 19], thickness [7, 19, 45] and temperature [18, 47] are relevant.

Table 3. List of auxiliary parameter values (to calculate simulation parameter values).

Parameter	Value
Total minimum element volume V_e (m ³)	1.00e - 07
Total minimum edge Δ_{\min} (m)	4.13e - 04
Total real simulation time t (s)	10
Critical time step glass (s) (Eq. 16)	2e6
Critical time step steel (s) (Eq. 16)	2e6
Critical time step PVB (s) (Eq. 16)	2e6
Overall Mesh size (m)	2.5e - 4
Mesh size projectile (m)	2.5e - 4
Mesh size plies (m)	2.5e - 4
Mesh size inter-layer (m)	2.5e - 4

Low velocity (≈ 20 m/s) hard impact experiments include the use of projectiles in form of road construction chippings [44], ballistics [9], drop-down weights [19, 32, 48], aluminum projectiles [48] and steel balls [6, 19, 49]. High velocity (around 180 m/s) soft impact experiments include the use of silicon rubber projectiles [43] and gas guns [18].

Wang et al [19] found that the panel size had an inferior effect on the breakage resistance [19]. Similarly, Monteleone et al [9] found that only a local area of the ply around the impact absorbed the impact energy for high velocities.

Karunarathna [45] found that impact velocity and plate thickness contributed significantly towards the impact resistance, compared to impact mass and inter-layer thickness. Wang et al [19] found an increased inter-layer thickness to have a negative effect on energy absorption. Liu et al [50] established that the inter-layer thickness did not contribute towards energy absorption. Behr and Kremer [49] found an increased inter-layer thickness to better protect the inner ply. Kim et al [51] numerically optimised the PVB inter-layer constitution to prevent all damage to the inner glass ply.

Liu et al [50] numerically investigated the optimisability of the inter-layer in terms of energy

absorption by simulating the impact of a human head. Zhang et al [47] investigated the influence of temperature on the inter-layer and found that a hybrid TPU/SGP/TPU inter-layer performed best over the entire range of tested temperatures.

4 COMPUTER SCIENCE APPROACH

The following data type macros are implemented in the code:

```

1 #define FLT float
2 #define INS int
3 #define DBL double
4 #define INT long
5 #define UCHR unsigned char
6 #define CHR char
7 #define UINT unsigned int
8 #define ULON unsigned long

```

Listing 1 Data type definitions

4.1 VTK format

The Visualisation Toolkit VTK [52] is an extremely popular open source software for graphic visualisation of scientific data. VTK APIs are available in many different programming languages and facilitate the generation of VTK files. Until now, the Y code included VTK API for programming language C to generate output files.

The required VTK version 5.8 library dependencies revealed themselves to be outdated and unobtainable online. All attempts by the author to obtain such a version for testing were not successful. Rewriting the code using a newer VTK version of the API would only temporarily solve this problem.

To diversify application to a wider range of operating systems, it was deemed necessary to hard code the output without using VTK libraries. Aside from the ill-documented official website [52], one of the only few reliable resources available was

deemed to be the Earth Models website by Bunge [53].

A complete implementation of the output algorithm can be found in file [Yod.c](#). In this section, an in-depth description of the different VTK formats and the algorithm is given.



Fig. 8. Snapshot of two rectangles moving apart from each other horizontally, at initial (top) and final time step (bottom).

For testing this VTK algorithm, a simple test setup was used consisting of two rectangular surfaces slowly moving apart from each other in the horizontal direction, as shown in Fig. 8.

4.2 VTK legacy file format

The VTK legacy file format is sufficiently documented (see [52]) and relatively easy to implement. On the downside, it only supports a minimal amount of features and is thus relatively inflexible.

Section 5 shows examples of VTK legacy output files. The header defines VTK version, file name, data encoding (ascii or binary) and dataset type¹⁴ [52].

The data is divided into sections including points, cells and cell types. The section header contains the keyword along with the total amount of entities of the section. The data is written continuously using spaces as separators. [52]

¹⁴here: unstructured grid

Every section has additional unique formatting rules. The points sections requires an additional data type identifier (here: `float`) to correctly identify the data of the coordinates [52]. The data in the cells section lists the node numbers of each element, appended to a number identifying the total amount of nodes of the element [52]. The cell type section identifies the geometric shape of each element, given by an index. Each index is written on a separate line. [52]

According to the specified data encoding option, the data may be encoded in decimal ascii or in binary.

```

1 void i2i64(FILE *fout, INS ib10)
2 {
3     putc((ib10 >> 56) & 0xFF, fout);
4     putc((ib10 >> 48) & 0xFF, fout);
5     putc((ib10 >> 40) & 0xFF, fout);
6     putc((ib10 >> 32) & 0xFF, fout);
7     putc((ib10 >> 24) & 0xFF, fout);
8     putc((ib10 >> 16) & 0xFF, fout);
9     putc((ib10 >> 8) & 0xFF, fout);
10    putc(ib10 & 0xFF, fout);
11 }

```

Listing 2 Function for binary encoding and outputting an int64

An example function which was used to encode the data to binary is given in List. 2. Decimals of different sizes are encoded accordingly. The `int64` \rightarrow input decimal `ib10` (size: 8 bytes) is encoded byte for byte, starting with the most significant byte. The byte order¹⁵ was assumed to be little endian, as operating systems with big endian were not available for testing.

For the algorithm, the fact was employed that the decimal is stored as a binary internally and the decimal can thus be treated as binary. First, the bytes are shifted to the beginning of the memory location of the decimal. A bit-wise comparison with $0xFF = 0b11111111 = 255$ then yields the value

¹⁵endianess

of the byte. This value is then encoded to a single character and printed to the output file via `putc`.

4.3 VTK XML file format

Compared to legacy files, XML files are much more difficult to implement. An examples are given in section 5.

The file is structured using nested keyword headers which are enclosed in angle brackets ("`<`" and "`>`"), according to XML language. Text indentation is not required but enhances readability.

Keyword headers are opened using `<keyword>` and closed using `</keyword>`. Keywords which do not contain any sub-keyword headers are opened and closed in one line using `<keyword\>`. Keyword headers usually contain additional mandatory and optional keywords in the format of `option="value"` [52].

The file header specifies versions, VTK file type and `byte_order` [52].

Depending on the specified `VTKFile` type, a unique set of sub-keyword headers is used. For the `Unstructured_Grid` VTK file type chosen here, the file content is structured using `<Piece>`. Within this header, it is required to specify the number of points and cells (elements) using `NumberOfPoints` and `NumberOfCells` \rightarrow [52].

`<Piece>` contains definition of `<Points>` and `<Cells>` \rightarrow , among other optional keyword sub-headers. `<Points>` expects exactly one `<DataArray>` containing the nodal coordinates. `<Cells>` expects one `<DataArray>` each for the cell connectivity (node configuration of each cell), the cell offsets (offsets in the cell connectivity list), as well as the cell type (cell shape index, see [52]) [53].

The data, listed after `<DataArray>` includes `type` (data type), `Name`, `NumberOfComponents`, `format`, `RangeMin` \rightarrow and `RangeMax`.

`RangeMin` and `RangeMax` indicate the minimal and maximal values of the data and are optional¹⁶. Simple array search functions were implemented in order to find the individual values.

`Name` specifies a unique name, enclosed by "", for the data set. The data array contained in `<Points>` requires no name. The data arrays enclosed by `<Cells>` require fixed names `Name="connectivity"`, `Name="offsets"` and `Name="types"` [52].

`format` specifies the encoding of the data.

In the case `format="ascii"`, the data is provided in decimal form, delimited by spaces, similar to section 4.2 [53]. Specifying an inappropriate data `type` for this format will not leave the data completely unusable, although induced type casting may yield unexpected results. The dependence on spaces as delimiters is highly impractical when transferring files between different operating systems and applications.

A more robust option is given by `format="binary"` \rightarrow ". Characters such as "<" (binary encoding of 0b00111100=d060) may potentially appear in binary encoded data. As these characters compose XML keyword headers, binary encoding is not realizable [53]. Thus, the data is encoded to base 64 (b64) (see 4.4).

For b64 encoding, a data header needs to be prepended to the data. The data header is always of type `int32` (data size: 4 bytes) and specifies the data size, i.e. the amount of binary bytes of subsequent data. The data size is not to be confused with the length of the printed b64 encoded data string in the output file, which is insignificant for now. The data size rather refers to the size of the binary data array in `bytes`, stored as specified by the datatype in the header. Specifying a data `type` of a different byte size for this format produces errors and renders the data useless.

¹⁶confirmed by tests

As an example, consider a `float32` array which contains 100 data values. The corresponding header is given by:

$$h = 100 \frac{32 \text{ bits}}{8 \text{ bits/byte}} = 400 \text{ bytes} \quad (19)$$

The header¹⁷ then needs to be encoded to b64, separately from the data. The encoded header string is immediately followed by the encoded data string, without any delimiters. Considering the fact that the data header type is fixed, the b64 encoded data header string length is always the same. Thus, no additional offset is necessary to specify the positional onset of the data after the data header [53].

Instead of supplying the data inline, it is possible to append data once, to an `<AppendedData>` section at the end of the file. This is achieved by specifying option `format="appended"` for each data array keyword header and providing an `offset` each time.

In doing so, the entire data is provided in a single long b64 encoded string, appended to an underscore "_". Like in the inline format, each encoded data string must be prepended by a b64 encoded header, which specifies the size of the following unencoded data section in bytes. The headers and the data sections are encoded separately each, without any delimiters between headers and data sections.

The offset value provided in each `<DataArray>` specifies the amount of bytes of unencoded data after the underscore to the beginning of the corresponding header. The method of evaluation of header offsets is illustrated in Tab. 4. The values in Tab. 4 are taken from an example file (see [53]), which is visualisable in Paraview.

In Tab. 4, the header offset of the first header is always 0. As the unencoded header is always an `int32` of size 4 bytes, the first data offset is 4. For a data array with 1926 values and data type size 8 bytes (e.g. `float64`), the data size in `bytes` amounts

¹⁷omitting the unit (bytes)

Table 4. Breakdown of offset values for an output file of a working example [53] with 642 points and 1280 cells. The desired (header) offsets are given in column 2.

Name	header offset	data offset	data size	data type size	values	components	points/cells
Points	0	4	15408	8	1926	3	642
Connectivity	15412	15416	15360	4	3840	3	1280
Offsets	30776	30780	5120	4	1280	1	1280
Types	35900	35904	1280	1	1280	1	1280
Points s	37184	37188	5136	8	642	1	642
Points v	42324	42328	15408	8	1926	3	642
Points n	57736	57740	15408	8	1926	3	642
Density	73148	73152	5136	8	642	1	642

to $1926 \cdot 8 \text{ bytes} = 15408 \text{ bytes}$. The number of values is comprised by the number of components and the number of points, i.e. $3 \cdot 642 = 1926$. The next header offset is evaluated by adding the data size to the data offset, i.e. $4 + 15408 = 15412$. The remaining offset values are evaluated accordingly.

4.4 Base 64 encoding

The output data consists of one- and two-dimensional **int** and **float** arrays containing nodal properties, elemental properties and flags. The computer stores the data in binary form, according to byte order (endianess) of the operating system at hand.

float numbers are usually stored in IEEE-754 format [54]. As the numbers are stored internally, the exact manner of storage is theoretically not significant as long as the position (the significance) of the bits in binary-stored **float** is not being violated.

As the base64 encoding function takes in a contiguous **CHR*** array, the data needs to be segmented into bytes. For the **INS** data header, this simply involves conversion from a 4-byte **int32** to 4 **CHR** bytes. The segmentation process for arrays is illustrated in Fig. 9. The array is segmented into single bytes, rearranged in groups of 3 bytes and again rearranged in groups of 6 bits. The 6-bit groups are encoded to characters and compose the encoded string.

As an example, the implementation approach is discussed by use of the 2-dimensional contact force array. In a first step, 2-dimensional arrays are reduced to contiguous one-dimensional arrays (List. 3).

```

1 DBL *cf; //contact force
2 INS i, j, k;
3 INS header;
4 header = sizeof(DBL) * ydn->nnopo * ydn->
   ↪ nnodim;
5 cf = malloc(header);
6 k = 0;
7 for (i = 0; i != ydn->nnopo; i++){
8   for (j = 0; j != ydn->nnodim; j++){
9     cf[k] = ydn->d2nfcon[j][i];
10    k++;}
11   cf[k] = ydn->d2nfcon[j][i];
12   k++;}

```

Listing 3 Converting 2-dimensional array to 1-dimensional array

In List. 3, **ydn->nnopo** denotes, in the class "**Y** database of **nodes**", the current **number of nodal points**. **ydn** **↪ ->nnodim** denotes the current **number of nodal dimensions** (2) and **ydn->d2nfcon** denotes the **double 2-dimensional nodal force of contact**.

As a result, the data is now stored in a contiguous one-dimensional array of **float64** and now needs to be segmented into bytes.

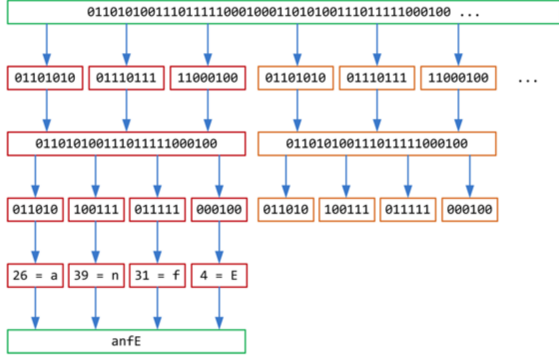


Fig. 9. Subsequent conversion of binary data to bytes, bit sextets, and encoded characters [55].

A first possible strategy is to apply simple data type casting, see List. 4.

```
1 FLT floats[4] = {1, 2, 3, 4}
2 //actual array is of variable size;
3 CHR *bytes = (CHR *) floats;
```

Listing 4 Segmentation approach via type casting with pointers

The `CHR* bytes` array could then be passed on to the encoding function. Test showed that this strategy seems to only work if the array to type cast does not contain any data before type casting. Thus, this approach is not appropriate here.

A second possible strategy is to declare a `union`, see List. 5.

```
1 union INTToCHR {
2     INS i;
3     CHR *c[sizeof(INS)];};
```

Listing 5 Segmentation approach via a union

Here, both `i` and `c` refer to the same location in memory. This approach potentially works for a single `float`. As the `CHR*` arrays would need to be concatenated dynamically, this approach is (according to the author's opinion) not appropriate either. Test which were carried out using this strategy

showed inconsistent outputs, indicating that the prompted data may not be contiguously stored.

A third strategy for dividing the data arrays into bytes uses a combination of `malloc` and `memcpy`, see List. 6.

```
1 CHR *bytes;
2 bytes = malloc(header);
3 memcpy(&bytes[0], cf, header);
```

Listing 6 Segmentation approach via memcpy

Testing confirmed that this method is successful. The `byte` array now contains the floats in contiguous order in binary form, stored as bytes.

The prepared data is passed to the base 64 encoding function `b64enc` in file `Yod.c`. The function takes some `CHR*` array `src` of length `len` as input, encodes it byte for byte and outputs character for character into the VTK output file `fout`.

The core of the algorithm (List. 7) was adopted from Malinen [56].

```
1 while (end - in > 2){
2     putc(enc[in[0] >> 2], fout);
3     putc(enc[((in[0] & 0x03) << 4) | (in[1] >>
4         ↪ 4)], fout);
5     putc(enc[((in[1] & 0x0f) << 2) | (in[2] >>
6         ↪ 6)], fout);
7     putc(enc[in[2] & 0x3f], fout);
8     in += 3;}
9
10 if (end - in){
11     putc(enc[in[0] >> 2], fout);
12     if (end - in == 1){
13         putc(enc[(in[0] & 0x03) << 4], fout);
14         putc('=', fout);}
15     else{
16         putc(enc[((in[0] & 0x03) << 4) | (in[1]
17             ↪ >> 4)], fout);
18         putc(enc[(in[1] & 0x0f) << 2], fout);}
19     putc('=', fout);}
20 return;
```

Listing 7 b64 algorithm

In List. 7, `in` and `end` are `CHR*` pointers which point to the beginning and end of the input array. Converting to base 64 requires rearranging the input in chunks of 6 bits. Each of these 6-bit chunks produces a value $v < 64 = 0b1000000$ and is able to be converted to one of 64 unique characters from the encoding array

```
CHR* enc = "ABCDEFGHIIJKLMNOPQRSTUVWXYZ"
"abcdefghijklmnopqrstuvwxyz0123456789+/" .
```

For every 3 bytes (or 24 bits), the algorithm produces 4 groups of 6 bits, i.e. 4 characters. The bits are extracted continuously via bit shifting. As mentioned before, the position or significance of the bits in the byte must not be violated. In other words, the value of the bit must not get lost through bit shifting. The algorithm is now explained in detail:

In line 2, the first 6 bits of the current character `in[0]` are extracted by bit shifting to produce the first 6-bit chunk. The value of this chunk is used to produce the index of the corresponding character in the encoding array `enc`.

The last two remaining bits of the current input character `in[0]` are evaluated and bit shifted in line 3 to account for the first 2 significant bits of the next 6-bit chunk. The 4 missing bits to complete the 6 bits are extracted from the first 4 bits of the second character `in[1]`, again by bit shifting.

In line 4, the 4 remaining bits from the second input character `in[1]` make up the first four bits of the next 6-bit chunk. The missing 2 bits of the 6-bit chunk are extracted from the third input character `in[2]`. This leaves 6 bits of the third input character remaining, making up another 6-bit chunk, as implemented in line 5.

If the input array length `len = end - in` is not divisible by 3, padding characters are required. The amount of padding depends on the amount of remaining input bytes to complete a group of three input bytes. If `len % 3 == 1`, two padding

characters '=' are appended to the encoded string. If `len % 3 == 2`, one padding character '=' is required. The algorithm is given in List. 7, lines 8-17.

Writing the output characters to a buffer instead of using `putc` reduces the amount of times of invoking the I/O buffer and may save computational time. This alternative was discarded as it did not provide any significant advantage in terms of computational costs in this minimal example.

5 RESULTS

5.1 Simulation

Fig. 10 shows snapshots of the simulation of a simple test geometry.

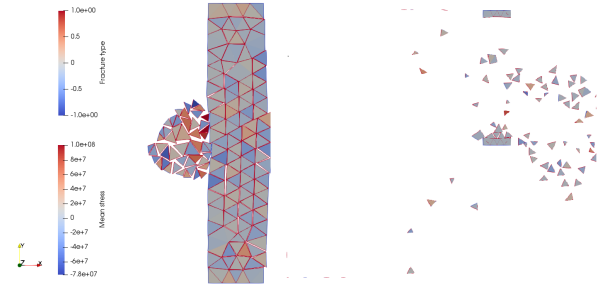


Fig. 10. Snapshots of simulation setup of a test geometry, at initial (left) and final time steps (right).

Fig. 11 shows a snapshot of the simulation of the final geometry.

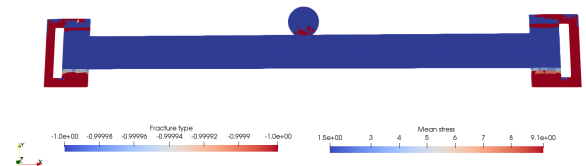


Fig. 11. Snapshot of simulation setup as described in section 3 at final time step

Table 5. Flags for producing different output in file `Yod.c`

flags	app	b10	b64	output
ym				Ym (original)
vtu_leg		1		legacy ascii
		0		legacy binary
vtu_xml	0	1		XML inline ascii
	0	0		XML inline base 64
	1		0	XML appended raw
	1		1	XML appended base

5.2 VTK implementation

Flags to switch between different output formats must be changed the code. As the output format for simulations will be fixed, input flags were not considered.

Flag `ym==1` generates the original `.ym` files. Alternatively, flags `vtu_leg==1` generates VTK `.vtu` legacy files, and `vtu_xml==1` generates VTK `.vtu` XML files.

For VTK legacy files, `b10==1` generates decimal ascii output, and `b10==0` generates binary output.

For VTK XML files, `app==1` generates appended output, while `app=0` generates inline output. For inline output, `b10==1` produces decimal ascii output, and `b10==0` produces base 64 encoded output. For appended output, `b64==1` generates base 64 encoded output, whereas `b64==0` creates raw binary encoded output.

A working example VTK legacy output file is given in List. 1. Working examples VTK XML b64 inline encoded output files are given in List. 3 and 4.

Some file formats are invalid for now. List. 2 shows an example of a VTK legacy file with binary encoding. List. 5 and 6 show examples of binary and base 64 encoded appended VTK XML output files. These examples are not visualisable in Paraview, presumably due to a bug in the algorithm.

```

1 # vtk DataFile Version 5.8
2 CODED
3 ASCII
4 DATASET UNSTRUCTURED_GRID
5 POINTS 20 float
6 -1.000000 1.000000 0.000000 1.000000 0.000000
  ↪ 1.000000 -1.000000 0.000000 0.000000
  ↪ 0.000000 0.000000 0.000000
7 1.000000 1.000000 1.000000 0.000000 0.000000
  ↪ -0.000000 0.000000 1.000000 -1.000001
  ↪ 0.000000 0.000000 1.000000
8 -1.000001 1.000000 -1.000001 0.000000 1.000001
  ↪ 1.000000 0.000000 1.000000 1.000001
  ↪ 0.000000 0.000000 -0.000000
9 1.000001 0.000000 0.000000 1.000000
10 CELLS 56
11 3 14 15 16
12 3 17 18 19
13 3 8 9 10
14 3 11 12 13
15 3 8 9 9
16 3 9 10 13
17 3 10 8 8
18 3 11 12 12
19 3 12 13 13
20 3 14 15 15
21 3 15 16 18
22 3 16 14 14
23 3 17 18 18
24 3 19 17 17
25 CELLTYPE 14
26 8
27 8
28 8
29 8
30 8
31 8
32 8
33 8
34 8
35 8
36 8
37 8
38 8
39 8

```

Listing 1. Example VTK legacy ascii encoded file

```

1 # vtk DataFile Version 5.8
2 CODED
3 ASCII
4 DATASET UNSTRUCTURED_GRID
5 POINTS 20 float
6 -1.000000 1.000000 0.000000 1.000000 0.000000
  ↪ 1.000000 -1.000000 0.000000 0.000000
  ↪ 0.000000 0.000000 0.000000
7 1.000000 1.000000 1.000000 0.000000 0.000000
  ↪ -0.000000 0.000000 1.000000 -1.000001
  ↪ 0.000000 0.000000 1.000000
8 -1.000001 1.000000 -1.000001 0.000000 1.000001
  ↪ 1.000000 0.000000 1.000000 1.000001
  ↪ 0.000000 0.000000 -0.000000
9 1.000001 0.000000 0.000000 1.000000
10 CELLS 56
11 3 14 15 16
12 3 17 18 19
13 3 8 9 10
14 3 11 12 13
15 3 8 9 9
16 3 9 10 13
17 3 10 8 8
18 3 11 12 12
19 3 12 13 13
20 3 14 15 15
21 3 15 16 18
22 3 16 14 14
23 3 17 18 18
24 3 19 17 17
25 CELLTYPE 14
26 8
27 8
28 8
29 8
30 8
31 8
32 8
33 8
34 8
35 8
36 8
37 8
38 8
39 8

```

Listing 2. Example VTK legacy binary encoded file

```

1 <?xml version="1.0"?>
2 <VTKFile type="UnstructuredGrid" version="0.1"
  ↪ byte_order = "LittleEndian">
3   <UnstructuredGrid>
4     <Piece NumberOfPoints="20"
      ↪ NumberOfCells="14">
5       <Points>
6         <DataArray type="Float32"
          ↪ NumberOfComponents="3"
          ↪ format="ascii" RangeMin="-1.000001"
          ↪ RangeMax="1.000001">
            -1.000000 1.000000 0 0.000000 1.000000
            ↪ 0 0.000000 1.000000 0 -1.000000
            ↪ 0.000000 0 0.000000 0.000000 0
            ↪ 0.000000 0.000000 0 1.000000
            ↪ 1.000000 0 1.000000 0.000000 0
            ↪ 0.000000 -0.000000 0 0.000000
            ↪ 1.000000 0 -1.000001 0.000000 0
            ↪ 0.000000 1.000000 0 -1.000001
            ↪ 1.000000 0 -1.000001 0.000000 0
            ↪ 1.000001 1.000000 0 0.000000
            ↪ 1.000000 0 1.000001 0.000000 0
            ↪ 0.000000 -0.000000 0 1.000001
            ↪ 0.000000 0 0.000000 1.000000 0
          </DataArray>
7       </Points>
8       <Cells>
9         <DataArray type="Int64"
          ↪ Name="connectivity"
          ↪ NumberOfComponents="1" RangeMin=""
          ↪ RangeMax="" format="ascii">
10           14 15 16 17 18 19 8 9 10 11 12 13 8 9 9
11           ↪ 9 10 13 10 8 8 11 12 12 12 13 13
12           ↪ 14 15 15 15 16 18 16 14 14 17 18
            ↪ 18 19 17 17
          </DataArray>
13       <DataArray type="UInt32" Name="offsets"
          ↪ NumberOfComponents="1" RangeMin=""
          ↪ RangeMax="" format="ascii">
14           3 6 9 12 15 18 21 24 27 30 33 36 39 42
15       </DataArray>
16       <DataArray type="UInt32" Name="types"
          ↪ NumberOfComponents="1" RangeMin=""
          ↪ RangeMax="" format="ascii">
17           5 5 5 5 5 5 5 5 5 5 5 5
18       </DataArray>
19     </Cells>
20   </Piece>
21 </UnstructuredGrid>
22 </VTKFile>
23

```

Listing 3. Example VTK XML file with decimal ascii inline encoding

```

14
15
16
17
18
19
20
21
22
23
1
2
3
4
5
6
7
8
9
10
11
12
13
<?xml version="1.0"?>
<VTKFile type="UnstructuredGrid" version="0.1"
  byte_order = "LittleEndian">
  <UnstructuredGrid>
    <Piece NumberOfPoints="20"
      NumberOfCells="14">
      <Points>
        <DataArray type="Float32"
          NumberOfComponents="3"
          format="binary"
          RangeMin="-1.000001"
          RangeMax="1.000001">
8AAAAA==AACAvwAagD8AAAAAAAAAAAAAgD8AAAA
  ↳ AAAAAAAAAAgD8AAAAAAAAACAvwAAAAAAAA
  ↳ AAAAAAAAAAAAAAAAAAAAAAAAAAAAAAAAAA
  ↳ AAACAPwAagD8AAAAAAAAACAPwAAAAAAAA
  ↳ AAAAAEdnLK0AAAAAAAAAAAAAgD8AAAA
  ↳ ACACAvwAAAAAAAAAAAAAAAgD8AAAA
  ↳ ACACAvwAagD8AAAAACACAvwAAAAAAAA
  ↳ ACACAPwAagD8AAAAAAAAAAAAAgD8AAAA
  ↳ ACACAPwAAAAAAAAAAAAEdnLK0AAAA
  ↳ ACACAPwAAAAAAAAAAAAAAAgD8AAAA
        </DataArray>
      </Points>
      <Cells>
        <DataArray type="Int64"
          Name="connectivity"
          NumberOfComponents="1" RangeMin=""
          RangeMax="" format="binary">
12 UAAAA==DgAAAAAAAAPAAAAAAAAABAAAAAAAA
  ↳ AEQAAAAAAAAASAAAAAAAAABMAAAAAAAAA
  ↳ ACAAAAAAAAAAJAAAAAAAAA0AAAAAAAA
  ↳ ACwAAAAAAAAMAAAAAAAAA0AAAAAAAA
  ↳ ACAAAAAAAAAAJAAAAAAAAAKAAAAAAAA
  ↳ ACQAAAAAAAAAKAAAAAAAAA0AAAAAAAA
  ↳ ACgAAAAAAAAIAAAAAAAAAAgAAAAAAAA
  ↳ ACwAAAAAAAAMAAAAAAAAAAwAAAAAAAA
  ↳ ADAAAAAAAAANAAAAAAAAA0AAAAAAAA
  ↳ ADgAAAAAAAAAPAAAAAAAAA8AAAAAAAA
  ↳ ADwAAAAAAAAQAAAAAAAAABIAAAAAAAAA
  ↳ AEAAAAAAAAAAOAAAAAAAAA4AAAAAAAA
  ↳ AEQAAAAAAAAASAAAAAAAAABIAAAAAAAAA
  ↳ AEwAAAAAAAARAAAAAAAAAABEAAAAAAAA
        </DataArray>
      </Cells>
    </Piece>
  </UnstructuredGrid>
</VTKFile>

```

```

<DataArray type="UInt32" Name="offsets"
  ↳ NumberOfComponents="1" RangeMin=""
  ↳ RangeMax="" format="binary">
0AAAAA==AwAAAAYAAAAJAAADAAAAA8AAAAASAA
  ↳ AAFQAAABgAAAAbAAAAHgAAACEAAAAkAA
  ↳ AAJwAAACoAAAA=
</DataArray>
<DataArray type="UInt32" Name="types"
  ↳ NumberOfComponents="1" RangeMin=""
  ↳ RangeMax="" format="binary">
0AAAAA==BQAAAAUAAAFAAAAABQAAAAUAAAFAA
  ↳ AABQAAAAUAAAFAAAAABQAAAAUAAAFAA
  ↳ AABQAAAAUAAAA=
</DataArray>
</Cells>
</Piece>
</UnstructuredGrid>
</VTKFile>

```

Listing 4. Example VTK XML file with b64 inline encoding

```

1
2
3
4
5
6
7
8
9
10
11
12
13
14
15
16
17
18
19
20
21
22
23
24
25
26
27
28
29
30
31
32
33
34
35
36
37
38
39
40
41
42
43
44
45
46
47
48
49
50
51
52
53
54
55
56
57
58
59
60
61
62
63
64
65
66
67
68
69
70
71
72
73
74
75
76
77
78
79
80
81
82
83
84
85
86
87
88
89
90
91
92
93
94
95
96
97
98
99
100
101
102
103
104
105
106
107
108
109
110
111
112
113
114
115
116
117
118
119
120
121
122
123
124
125
126
127
128
129
130
131
132
133
134
135
136
137
138
139
140
141
142
143
144
145
146
147
148
149
150
151
152
153
154
155
156
157
158
159
160
161
162
163
164
165
166
167
168
169
170
171
172
173
174
175
176
177
178
179
180
181
182
183
184
185
186
187
188
189
190
191
192
193
194
195
196
197
198
199
200
201
202
203
204
205
206
207
208
209
210
211
212
213
214
215
216
217
218
219
220
221
222
223
224
225
226
227
228
229
230
231
232
233
234
235
236
237
238
239
240
241
242
243
244
245
246
247
248
249
250
251
252
253
254
255
256
257
258
259
260
261
262
263
264
265
266
267
268
269
270
271
272
273
274
275
276
277
278
279
280
281
282
283
284
285
286
287
288
289
290
291
292
293
294
295
296
297
298
299
300
301
302
303
304
305
306
307
308
309
310
311
312
313
314
315
316
317
318
319
320
321
322
323
324
325
326
327
328
329
330
331
332
333
334
335
336
337
338
339
340
341
342
343
344
345
346
347
348
349
350
351
352
353
354
355
356
357
358
359
360
361
362
363
364
365
366
367
368
369
370
371
372
373
374
375
376
377
378
379
380
381
382
383
384
385
386
387
388
389
390
391
392
393
394
395
396
397
398
399
400
401
402
403
404
405
406
407
408
409
410
411
412
413
414
415
416
417
418
419
420
421
422
423
424
425
426
427
428
429
430
431
432
433
434
435
436
437
438
439
440
441
442
443
444
445
446
447
448
449
450
451
452
453
454
455
456
457
458
459
460
461
462
463
464
465
466
467
468
469
470
471
472
473
474
475
476
477
478
479
480
481
482
483
484
485
486
487
488
489
490
491
492
493
494
495
496
497
498
499
500
501
502
503
504
505
506
507
508
509
510
511
512
513
514
515
516
517
518
519
520
521
522
523
524
525
526
527
528
529
530
531
532
533
534
535
536
537
538
539
540
541
542
543
544
545
546
547
548
549
550
551
552
553
554
555
556
557
558
559
560
561
562
563
564
565
566
567
568
569
570
571
572
573
574
575
576
577
578
579
580
581
582
583
584
585
586
587
588
589
590
591
592
593
594
595
596
597
598
599
600
601
602
603
604
605
606
607
608
609
610
611
612
613
614
615
616
617
618
619
620
621
622
623
624
625
626
627
628
629
630
631
632
633
634
635
636
637
638
639
640
641
642
643
644
645
646
647
648
649
650
651
652
653
654
655
656
657
658
659
660
661
662
663
664
665
666
667
668
669
670
671
672
673
674
675
676
677
678
679
680
681
682
683
684
685
686
687
688
689
690
691
692
693
694
695
696
697
698
699
700
701
702
703
704
705
706
707
708
709
710
711
712
713
714
715
716
717
718
719
720
721
722
723
724
725
726
727
728
729
730
731
732
733
734
735
736
737
738
739
740
741
742
743
744
745
746
747
748
749
750
751
752
753
754
755
756
757
758
759
760
761
762
763
764
765
766
767
768
769
770
771
772
773
774
775
776
777
778
779
780
781
782
783
784
785
786
787
788
789
790
791
792
793
794
795
796
797
798
799
800
801
802
803
804
805
806
807
808
809
810
811
812
813
814
815
816
817
818
819
820
821
822
823
824
825
826
827
828
829
830
831
832
833
834
835
836
837
838
839
840
841
842
843
844
845
846
847
848
849
850
851
852
853
854
855
856
857
858
859
860
861
862
863
864
865
866
867
868
869
870
871
872
873
874
875
876
877
878
879
880
881
882
883
884
885
886
887
888
889
890
891
892
893
894
895
896
897
898
899
900
901
902
903
904
905
906
907
908
909
910
911
912
913
914
915
916
917
918
919
920
921
922
923
924
925
926
927
928
929
930
931
932
933
934
935
936
937
938
939
940
941
942
943
944
945
946
947
948
949
950
951
952
953
954
955
956
957
958
959
960
961
962
963
964
965
966
967
968
969
970
971
972
973
974
975
976
977
978
979
980
981
982
983
984
985
986
987
988
989
990
991
992
993
994
995
996
997
998
999
1000
1001
1002
1003
1004
1005
1006
1007
1008
1009
1010
1011
1012
1013
1014
1015
1016
1017
1018
1019
1020
1021
1022
1023
1024
1025
1026
1027
1028
1029
1030
1031
1032
1033
1034
1035
1036
1037
1038
1039
1040
1041
1042
1043
1044
1045
1046
1047
1048
1049
1050
1051
1052
1053
1054
1055
1056
1057
1058
1059
1060
1061
1062
1063
1064
1065
1066
1067
1068
1069
1070
1071
1072
1073
1074
1075
1076
1077
1078
1079
1080
1081
1082
1083
1084
1085
1086
1087
1088
1089
1090
1091
1092
1093
1094
1095
1096
1097
1098
1099
1100
1101
1102
1103
1104
1105
1106
1107
1108
1109
1110
1111
1112
1113
1114
1115
1116
1117
1118
1119
1120
1121
1122
1123
1124
1125
1126
1127
1128
1129
1130
1131
1132
1133
1134
1135
1136
1137
1138
1139
1140
1141
1142
1143
1144
1145
1146
1147
1148
1149
1150
1151
1152
1153
1154
1155
1156
1157
1158
1159
1160
1161
1162
1163
1164
1165
1166
1167
1168
1169
1170
1171
1172
1173
1174
1175
1176
1177
1178
1179
1180
1181
1182
1183
1184
1185
1186
1187
1188
1189
1190
1191
1192
1193
1194
1195
1196
1197
1198
1199
1200
1201
1202
1203
1204
1205
1206
1207
1208
1209
1210
1211
1212
1213
1214
1215
1216
1217
1218
1219
1220
1221
1222
1223
1224
1225
1226
1227
1228
1229
1230
1231
1232
1233
1234
1235
1236
1237
1238
1239
1240
1241
1242
1243
1244
1245
1246
1247
1248
1249
1250
1251
1252
1253
1254
1255
1256
1257
1258
1259
1260
1261
1262
1263
1264
1265
1266
1267
1268
1269
1270
1271
1272
1273
1274
1275
1276
1277
1278
1279
1280
1281
1282
1283
1284
1285
1286
1287
1288
1289
1290
1291
1292
1293
1294
1295
1296
1297
1298
1299
1300
1301
1302
1303
1304
1305
1306
1307
1308
1309
1310
1311
1312
1313
1314
1315
1316
1317
1318
1319
1320
1321
1322
1323
1324
1325
1326
1327
1328
1329
1330
1331
1332
1333
1334
1335
1336
1337
1338
1339
1340
1341
1342
1343
1344
1345
1346
1347
1348
1349
1350
1351
1352
1353
1354
1355
1356
1357
1358
1359
1360
1361
1362
1363
1364
1365
1366
1367
1368
1369
1370
1371
1372
1373
1374
1375
1376
1377
1378
1379
1380
1381
1382
1383
1384
1385
1386
1387
1388
1389
1390
1391
1392
1393
1394
1395
1396
1397
1398
1399
1400
1401
1402
1403
1404
1405
1406
1407
1408
1409
1410
1411
1412
1413
1414
1415
1416
1417
1418
1419
1420
1421
1422
1423
1424
1425
1426
1427
1428
1429
1430
1431
1432
1433
1434
1435
1436
1437
1438
1439
1440
1441
1442
1443
1444
1445
1446
1447
1448
1449
1450
1451
1452
1453
1454
1455
1456
1457
1458
1459
1460
1461
1462
1463
1464
1465
1466
1467
1468
1469
1470
1471
1472
1473
1474
1475
1476
1477
1478
1479
1480
1481
1482
1483
1484
1485
1486
1487
1488
1489
1490
1491
1492
1493
1494
1495
1496
1497
1498
1499
1500
1501
1502
1503
1504
1505
1506
1507
1508
1509
1510
1511
1512
1513
1514
1515
1516
1517
1518
1519
1520
1521
1522
1523
1524
1525
1526
1527
1528
1529
1530
1531
1532
1533
1534
1535
1536
1537
1538
1539
1540
1541
1542
1543
1544
1545
1546
1547
1548
1549
1550
1551
1552
1553
1554
1555
1556
1557
1558
1559
1560
1561
1562
1563
1564
1565
1566
1567
1568
1569
1570
1571
1572
1573
1574
1575
1576
1577
1578
1579
1580
1581
1582
1583
1584
1585
1586
1587
1588
1589
1590
1591
1592
1593
1594
1595
1596
1597
1598
1599
1600
1601
1602
1603
1604
1605
1606
1607
1608
1609
1610
1611
1612
1613
1614
1615
1616
1617
1618
1619
1620
1621
1622
1623
1624
1625
1626
1627
1628
1629
1630
1631
1632
1633
1634
1635
1636
1637
1638
1639
1640
1641
1642
1643
1644
1645
1646
1647
1648
1649
1650
1651
1652
1653
1654
1655
1656
1657
1658
1659
1660
1661
1662
1663
1664
1665
1666
1667
1668
1669
1670
1671
1672
1673
1674
1675
1676
1677
1678
1679
1680
1681
1682
1683
1684
1685
1686
1687
1688
1689
1690
1691
1692
1693
1694
1695
1696
1697
1698
1699
1700
1701
1702
1703
1704
1705
1706
1707
1708
1709
1710
1711
1712
1713
1714
1715
1716
1717
1718
1719
1720
1721
1722
1723
1724
1725
1726
1727
1728
1729
1730
1731
1732
1733
1734
1735
1736
1737
1738
1739
1740
1741
1742
1743
1744
1745
1746
1747
1748
1749
1750
1751
1752
1753
1754
1755
1756
1757
1758
1759
1760
1761
1762
1763
1764
1765
1766
1767
1768
1769
1770
1771
1772
1773
1774
1775
1776
1777
1778
1779
1780
1781
1782
1783
1784
1785
1786
1787
1788
1789
1790
1791
1792
1793
1794
1795
1796
1797
1798
1799
1800
1801
1802
1803
1804
1805
1806
1807
1808
1809
1810
1811
1812
1813
1814
1815
1816
1817
1818
1819
1820
1821
1822
1823
1824
1825
1826
1827
1828
1829
1830
1831
1832
1833
1834
1835
1836
1837
1838
1839
1840
1841
1842
1843
1844
1845
1846
1847
1848
1849
1850
1851
1852
1853
1854
1855
1856
1857
1858
1859
1860
1861
1862
1863
1864
1865
1866
1867
1868
1869
1870
1871
1872
1873
1874
1875
1876
1877
1878
1879
1880
1881
1882
1883
1884
1885
1886
1887
1888
1889
1890
1891
1892
1893
1894
1895
1896
1897
1898
1899
1900
1901
1902
1903
1904
1905
1906
1907
1908
1909
1910
1911
1912
1913
1914
1915
1916
1917
1918
1919
1920
1921
1922
1923
1924
1925
1926
1927
1928
1929
1930
1931
1932
1933
1934
1935
1936
1937
1938
1939
1940
1941
1942
1943
1944
1945
1946
1947
1948
1949
1950
1951
1952
1953
1954
1955
1956
1957
1958
1959
1960
1961
1962
1963
1964
1965
1966
1967
1968
1969
1970
1971
1972
1973
1974
1975
1976
1977
1978
1979
1980
1981
1982
1983
1984
1985
1986
1987
1988
1989
1990
1991
1992
1993
1994
1995
1996
1997
1998
1999
2000
2001
2002
2003
2004
2005
2006
2007
2008
2009
2010
2011
2012
2013
2014
2015
2016
2017
2018
2019
2020
2021
2022
2023
2024
2025
2026
2027
2028
2029
2030
2031
2032
2033
2034
2035
2036
2037
2038
2039
2040
2041
2042
2043
2044
2045
2046
2047
2048
2049
2050
2051
2052
2053
2054
2055
2056
2057
2058
2059
2060
2061
2062
2063
2064
2065
2066
2067
2068
2069
2070
2071
2072
2073
2074
2075
2076
2077
2078
2079
2080
2081
2082
2083
2084
2085
2086
2087
2088
2089
2090
2091
2092
2093
2094
2095
2096
2097
2098
2099
2100
2101
2102
2103
2104
2105
2106
2107
2108
2109
2110
2111
2112
2113
2114
2115
2116
2117
2118
2119
2120
2121
2122
2123
2124
2125
2126
2127
2128
2129
2130
2131
2132
2133
2134
2135
2136
2137
2138
2139
2140
2141
2142
2143
2144
2145
2146
2147
2148
2149
2150
2151
2152
2153
2154
2155
2156
2157
2158
2159
2160
2161
2162
2163
2164
2165
2166
2167
2168
2169
2170
2171
2172
2173
2174
2175
2176
2177
2178
2179
2180
2181
2182
2183
2184
2185
2186
2187
2188
2189
2190
2191
2192
2193
2194
2195
2196
2197
2198
2199
2200
2201
2202
2203
2204
2205
2206
2207
2208
2209
2210
2211
2212
2213
2214
2215
2216
2217
2218
2219
2220
2221
2222
2223
2224
2225
2226
2227
2228
2229
2230
2231
2232
2233
2234
2235
2236
2237
2238
2239
2240
2241
2242
2243
2244
2245
2246
2247
2248
2249
2250
2251
2252
2253
2254
2255
2256
2257
2258
2259
2260
2261
2262
2263
2264
2265
2266
2267
2268
2269
2270
2271
2272
2273
2274
2275
2276
2277
2278
2279
2280
2281
2282
2283
2284
2285
2286
2287
2288
2289
2290
2291
2292
2293
2294
2295
2296
2297
2298
2299
2300
2301
2302
2303
2304
2305
2306
2307
2308
2309
2310
2311
2312
2313
2314
2315
2316
2317
2318
2319
2320
2321
2322
2323
2324
2325
2326
2327
2328
2329
2330
2331
2332
2333
2334
2335
2336
2337
2338
2339
2340
2341
2342
2343
2344
2345
2346
2347
2348
2349
2350
2351
2352
2353
2354
2355
2356
2357
2358
2359
2360
2361
2362
2363
2364
2365
2366
2367
2368
2369
2370
2371
2372
2373
2374
2375
2376
2377
2378
2379
2380
2381
2382
2383
2384
2385
2386
2387
2388
2389
2390
2391
2392
2393
2394
2395
2396
2397
2398
2399
2400
2401
2402
2403
2404
2405
2406
2407
2408
2409
2410
2411
2412
2413
2414
2415
2416
2417
2418
2419
2420
2421
2422
2423
2424
2425
2426
2427
2428
2429
2430
2431
2432
2433
2434
2435
2436
2437
2438
2439
2440
2441
2442
2443
2444
2445
2446
2447
2448
2449
2450
2451
2452
2453
2454
2455
2456
2457
2458
2459
2460
2461
2462
2463
2464
2465
2466
2467
2468
2469
2470
2471
2472
2473
2474
2475
2476
2477
2478
2479
2480
2481
2482
2483
2484
2485
2486
2487
```

<pre> 11 <DataArray type="Int64" ↪ Name="connectivity" ↪ NumberOfComponents="1" RangeMin="" ↪ RangeMax="" format="binary"> 12 UAEAAA==DgAAAAAAAAAAAAAAAAABAAAAAAAA ↪ AEQAAAAAAAAASAAAAAAAAABMAAAAAAAAA ↪ AAAAAAAAAAJAAAAAAAAAoAAAAAAAA ↪ ACwAAAAAAAAMAAAAAAAAA0AAAAAAAA ↪ AAAAAAAAAAJAAAAAAAAAKAAAAAAAA ↪ ACQAAAAAAAAKAAAAAAAAA0AAAAAAAA ↪ ACgAAAAAAAAIAAAAAAAAAAgAAAAAAAA ↪ ACwAAAAAAAAMAAAAAAAAAAwAAAAAAAA ↪ ADAAAAAAAAAAAAAAAAA0AAAAAAAA ↪ ADgAAAAAAAAPAAAAAAAAA8AAAAAAAA ↪ ADwAAAAAAAAQAAAAAAAAABIAAAAAAAAA ↪ AEAAAAAAAAA0AAAAAAAAA4AAAAAAAA ↪ AEQAAAAAAAAASAAAAAAAAABIAAAAAAAAA ↪ AEwAAAAAAAARAAAAAAAAAABEAAAAAAAA 13 </DataArray> 14 <DataArray type="UInt32" Name="offsets" ↪ NumberOfComponents="1" RangeMin="" ↪ RangeMax="" format="binary"> 15 OAAAAA==AwAAAAAYAAAAJAAAAADAAAAA8AAAAA ↪ AAFQAAABgAAAAbAAAAAHgAAACEAAAAKAA ↪ AAJwAAACoAAAA= 16 </DataArray> 17 <DataArray type="UInt32" Name="types" ↪ NumberOfComponents="1" RangeMin="" ↪ RangeMax="" format="binary"> 18 OAAAAA==BQAAAAUAAAFAAAAABQAAAAUAAAF ↪ AABQAAAAUAAAFAAAAABQAAAAUAAAF ↪ AABQAAAAUAAAA= 19 </DataArray> 20 </Cells> 21 </Piece> 22 </UnstructuredGrid> 23 </VTKFile> </pre>	<pre> 6 7 8 9 10 11 12 13 14 15 16 17 18 19 </pre>	<pre> <DataArray type="Float32" ↪ NumberOfComponents="3" ↪ format="binary" ↪ RangeMin="-1.000001" ↪ RangeMax="1.000001"> 8AAAAA==AACAvwAagD8AAAAAAAAAAAAAgD8AAAA ↪ AAAAAAAAgD8AAAAAACAvwAAAAAAAA ↪ AAAAAAAAAAAAAAAAAAAAAAAAAAAAA ↪ AAACAPwAagD8AAAAAACAPwAAAAAAAA ↪ AAAAAEdnLK0AAAAAAAAAAAAAgD8AAAA ↪ ACACAvwAAAAAAAAAAAAAAAgD8AAAA ↪ ACACAvwAagD8AAAAACACAvwAAAAAAAA ↪ ACACAPwAagD8AAAAAACAPwAAAAAAAA ↪ ACACAPwAAAAAAAAAAAAEdnLK0AAAA ↪ ACACAPwAAAAAAAAAAAAAAAgD8AAAA </DataArray> </Points> <Cells> <DataArray type="Int64" ↪ Name="connectivity" ↪ NumberOfComponents="1" RangeMin="" ↪ RangeMax="" format="binary"> UAEAAA==DgAAAAAAAAAAAAAAAAABAAAAAAAA ↪ AEQAAAAAAAAASAAAAAAAAABMAAAAAAAAA ↪ AAAAAAAAAAJAAAAAAAAAoAAAAAAAA ↪ ACwAAAAAAAAMAAAAAAAAA0AAAAAAAA ↪ AAAAAAAAAAJAAAAAAAAAKAAAAAAAA ↪ ACQAAAAAAAAKAAAAAAAAA0AAAAAAAA ↪ ACgAAAAAAAAIAAAAAAAAAAgAAAAAAAA ↪ ACwAAAAAAAAMAAAAAAAAAAwAAAAAAAA ↪ ADAAAAAAAAAAAAAAAAA0AAAAAAAA ↪ ADgAAAAAAAAPAAAAAAAAA8AAAAAAAA ↪ ADwAAAAAAAAQAAAAAAAAABIAAAAAAAAA ↪ AEAAAAAAAAA0AAAAAAAAA4AAAAAAAA ↪ AEQAAAAAAAAASAAAAAAAAABIAAAAAAAAA ↪ AEwAAAAAAAARAAAAAAAAAABEAAAAAAAA </DataArray> <DataArray type="UInt32" Name="offsets" ↪ NumberOfComponents="1" RangeMin="" ↪ RangeMax="" format="binary"> OAAAAA==AwAAAAAYAAAAJAAAAADAAAAA8AAAAA ↪ AAFQAAABgAAAAbAAAAAHgAAACEAAAAKAA ↪ AAJwAAACoAAAA= </DataArray> <DataArray type="UInt32" Name="types" ↪ NumberOfComponents="1" RangeMin="" ↪ RangeMax="" format="binary"> OAAAAA==BQAAAAUAAAFAAAAABQAAAAUAAAF ↪ AABQAAAAUAAAFAAAAABQAAAAUAAAF ↪ AABQAAAAUAAAA= </DataArray> </Cells> </Piece> </UnstructuredGrid> </VTKFile> </pre>
---	--	---

Listing 5. Example VTK XML file with b64 inline encoding

<pre> 1 <?xml version="1.0"?> 2 <VTKFile type="UnstructuredGrid" version="0.1" ↪ byte_order = "LittleEndian"> 3 <UnstructuredGrid> 4 <Piece NumberOfPoints="20" ↪ NumberOfCells="14"> 5 <Points> </pre>	<pre> 15 16 17 18 19 </pre>	<pre> </DataArray> <DataArray type="UInt32" Name="types" ↪ NumberOfComponents="1" RangeMin="" ↪ RangeMax="" format="binary"> OAAAAA==BQAAAAUAAAFAAAAABQAAAAUAAAF ↪ AABQAAAAUAAAFAAAAABQAAAAUAAAF ↪ AABQAAAAUAAAA= </DataArray> </Cells> </Piece> </UnstructuredGrid> </VTKFile> </pre>
---	-----------------------------	--

```

20     </Cells>
21 </Piece>
22 </UnstructuredGrid>
23 </VTKFile>

```

Listing 6. Example VTK XML file with b64 inline encoding

6 DISCUSSION

6.1 Simulation

The simulation clearly only produces realistic results for simple geometry setups.

Simulation results for more complex geometries are not realistic. Here, the projectile of prescribed material steel locally deforms on impact on the glass, while the glass ply does not show any reaction to the impact. Due to these unrealistic results, none of the findings from previous research could be confirmed.

The simulation might have failed due to errors in the pre-processing software.

The pre-processor GID appeared to be faulty. The prepared input Y file presumably contained definitions which are contradicted in the Y2D code. For example, the nodes which make up each element may have been defined in the opposite rotational direction GID. It may be possible that this error may have been caused by importing geometries from AutoCAD. This error may be connected to a potential inconsistency in applied operating systems, i.e. the preprocessor may have produced different outputs on different operating systems. As code for these programs is not publicly available, which makes further investigation difficult to impossible.

As the pre-processor GID seems to be unpredictable, it is of significant importance to replace this software with more reliable alternatives such as Gmesh [57]. Alternatively, an algorithm could be implemented as part of the Y2D code which could check the validity of the input Y file.

The problem may also be located in the original Y2D code, made by previous programmers. Running the code in a clean environment using for instance Travis CI results in errors. This fact strongly indicates that errors in the code are a likely cause for the simulation to fail.

```

1 JCS0=d1pjcs[propID];

```

Listing 8 Memory allocation error for variable JCS0 in file Yrd.c

One such error occurs in line 676 in file Yrd.c, see List. 8. The variable JCS0 is reserved for rock materials, which are not applied in this paper. There seems to be a memory allocation error, although the circumstances are not quite clear to the author.

Another error occurs at the beginning of the program in line 733 in file Yrd.c, see List. 9.

```

1 #define SETLINEBUF(fcheck) setvbuf((fcheck),
    ↪ NULL, _IONBF, 0); //definition
2 SETLINEBUF(ydc->fcheck); //line 733

```

Listing 9 SETLINEBUF Error in file Yrd.c

The command `setvbuf((fcheck), NULL, _IONBF, ↪ 0)` presumably assigns an empty buffer `NULL` to some file `ydc->fcheck`. However, the specifics and the purpose of this command are again unclear to the author.

6.2 VTK Implementation

The results have a significant impact on further development of the FEMDEM code. Before, the Y2D code needed to be run on remote servers. Specifically, this involved submitting jobs each time via the HPC system. Debugging proved to be extremely inconvenient and inefficient, as error files from failed jobs generally do not specify the exact position or kind of error.

Code using VTK libraries to produce the output was replaced by an elementary implementation. VTK output files are now able to be generated and simulated without additional dependencies. Removing the VTK module allows the code to be able to be run locally.

The current algorithm needs to be further improved and adjusted. As tests were conducted using a simple setup without fracturing, joint elements need to be visualised accordingly. The following output file types are still faulty:

- (1) binary output for VTK legacy files
- (2) appended output for VTK XML files

The output algorithm may be further improved by the implementation of a compression algorithm to compress to the VTK XML files. This is indicated in the file by adding the option

```
compressor="vtkZlibDataCompressor"
```

to the header [52]. Bunge [53] provides a promising algorithm, but it remains to be revised, adjusted and implemented.

Most significantly, the modified code paves the way for program debugging and testing. Possible software for debugging on Linux Ubuntu operating system includes the GNU Project Debugger gdb (url: <https://www.gnu.org/software/gdb/>). Debugging is necessary until the code runs in a clean environment.

Once the code is debugged, additional features may be implemented in the code. One such feature includes inserting joint elements between elements of different materials. This would be particularly of interest for glass, considering the interface interaction between glass and the PVB inter-layer. Another future task is to implement a model for this inter-layer based on hyper-elastic laws.

The results can also be applied to the Y3D code to simulate three-dimensional output. The algorithm to generate three-dimensional output code is estimated to be of similar nature as for the Y2D code. It is expected that only minor adjustments to the algorithm are necessary.

It should only be necessary to involve the HPC system once the debugging and testing is finished. Sensible applications involving the HPC system include simulations on a larger scale.

ACKNOWLEDGMENTS

Special gratitude pertains to the Research Computing Service RCS at Imperial College for their constant support throughout the project. The author would also like to thank course director Dr Gerard Gorman¹⁸ and course administrator Ying Ashton¹⁹ for support during this research. Finally, the author would like to thank the project coordinators, and the supervisors for enabling this project.

REFERENCES

- [1] A. Stolz, O. Millon, C. Bedon, C. Kevin, A. V. Doormaal, C. Haberacker, M. Larcher, E. Commission, O. Millon, A. Saarenheimo, G. Solomos, E. Commission, and A. Stolz. 2015. *Recommendations for the Improvement of Existing European Norms for Testing the Resistance of Windows and Glazed Façades to Explosive Effects*. ISBN: 9789279533945. DOI: <https://doi.org/10.2788/319252>. <https://ec.europa.eu/jrc/en/publication/recommendations-improvement-existing-european-norms-testing-resistance-windows-and-glazed-facades> (cited on pages 1, 6).

¹⁸g.gorman@imperial.ac.uk, Imperial College London, Department of Earth and Science

¹⁹y.ashton@imperial.ac.uk, Imperial College London, Department of Earth and Science

- [2] M. A. Samieian, D. Cormie, D. Smith, W. Wholley, B. R. Blackman, J. P. Dear, and P. A. Hooper. 2019. On the bonding between glass and PVB in laminated glass. *Engineering Fracture Mechanics*, 214, April, 504–519. ISSN: 00137944. DOI: <https://doi.org/10.1016/j.engfracmech.2019.04.006>. <https://doi.org/10.1016/j.engfracmech.2019.04.006> (cited on pages 1, 3).
- [3] W. Xu and M. Zang. 2014. Four-point combined DE/FE algorithm for brittle fracture analysis of laminated glass. *International Journal of Solids and Structures*, 51, 10, (May 2014), 1890–1900. ISSN: 00207683. DOI: <https://doi.org/10.1016/j.ijsolstr.2014.01.026> (cited on pages 1, 3).
- [4] C. D. Wu, X. Q. Yan, and L. M. Shen. 2014. A numerical study on dynamic failure of nano-material enhanced laminated glass under impact. In *IOP Conference Series: Materials Science and Engineering* number 1. Volume 10. Institute of Physics Publishing. DOI: <https://doi.org/10.1088/1757-899X/10/1/012176> (cited on pages 1, 2, 7, 8).
- [5] S. Chen, M. Zang, D. Wang, S. Yoshimura, and T. Yamada. 2017. Numerical analysis of impact failure of automotive laminated glass: A review. (August 2017). DOI: <https://doi.org/10.1016/j.compositesb.2017.04.007> (cited on page 1).
- [6] F. W. Flocker and L. R. Dharani. 1998. Modeling interply debonding in laminated architectural glass subject to low velocity impact. *Structural Engineering and Mechanics*, 6, 5, 485–496. ISSN: 12254568. DOI: <https://doi.org/10.12989/sem.1998.6.5.485> (cited on pages 1, 8).
- [7] F. S. Ji, L. R. Dharani, and R. A. Behr. 1998. Damage probability in laminated glass subjected to low velocity small missile impacts. *Journal of Materials Science*, 33, 19, 4775–4782. ISSN: 00222461. DOI: <https://doi.org/10.1023/A:1004457624817> (cited on pages 1, 8).
- [8] X. Brajer, F. Hild, and S. Roux. 2010. On the dynamic fragmentation of glass: A meso-damage model. *International Journal of Fracture*, 163, 1-2, (May 2010), 121–131. ISSN: 03769429. DOI: <https://doi.org/10.1007/s10704-009-9421-9> (cited on pages 1, 8).
- [9] L. Monteleone, R. Steindler, and G. Kajon. 2004. Monitored ballistic tests on shockproof sandwich glasses in different conditions. *Experimental Techniques*, 28, 5, 28–32. ISSN: 07328818. DOI: <https://doi.org/10.1111/j.1747-1567.2004.tb00183.x> (cited on pages 1, 8).
- [10] L. Biolzi, S. Cattaneo, and G. Rosati. 2010. Progressive damage and fracture of laminated glass beams. *Construction and Building Materials*, 24, 4, 577–584. ISSN: 09500618. DOI: <https://doi.org/10.1016/j.conbuildmat.2009.09.007> (cited on page 1).
- [11] P. J. G. Schreurs. 2012. Fracture Mechanics. Eindhoven, (September 2012). <http://www.mate.tue.nl/~piet/edu/frm/pdf/frmsyl1213.pdf> (cited on page 1).
- [12] A. Munjiza, K. R. F. Andrews, and J. K. White. 1999. Combined single and smeared crack model in combined finite-discrete element analysis. *International Journal for Numerical Methods in Engineering*, 44, 1, (January 1999), 41–57. ISSN: 00295981. DOI: [https://doi.org/10.1002/\(SICI\)1097-0207\(19990110\)44:1<41::AID-NME487>3.0.CO;2-A](https://doi.org/10.1002/(SICI)1097-0207(19990110)44:1<41::AID-NME487>3.0.CO;2-A) (cited on pages 2, 3).
- [13] J. P. Latham, J. Xiang, A. Farsi, C. Joulin, N. Karantzoulis, A. Obeysekara, and P. Yang. 2019. Solidity Website. (2019). <http://solidityproject.com/> (cited on pages 2, 4).
- [14] A. Munjiza. 2004. *The Combined Finite-Discrete Element Method*. English. John Wiley & Sons, Ltd, Hoboken, 350. ISBN: 0470841990. DOI: <https://doi.org/10.1002/0470020180>. <https://onlinelibrary.wiley.com/doi/book/10.1002/0470020180> (cited on pages 2–5).
- [15] M. Abuaisha, D. W. Eaton, J. Priest, and R. Wong. 2015. Finite / Discrete Element Method

- (FDEM) by Y- Geo : An overview. *Micro-seismic Industry Consortium*, 5, February, 13. https://www.researchgate.net/publication/295705226_FiniteDiscrete_Element_Method_FDEM_by_Y-Geo_An_overview (cited on page 2).
- [16] Q. Lei, J. P. Latham, and J. Xiang. 2016. Implementation of an Empirical Joint Constitutive Model into Finite-Discrete Element Analysis of the Geomechanical Behaviour of Fractured Rocks. *Rock Mechanics and Rock Engineering*, 49, 12, (December 2016), 4799–4816. ISSN: 0723-2632. DOI: <https://doi.org/10.1007/s00603-016-1064-3>. <http://link.springer.com/10.1007/s00603-016-1064-3> (cited on pages 2, 4).
- [17] X. Chen and A. H. Chan. 2018. Modelling impact fracture and fragmentation of laminated glass using the combined finite-discrete element method. *International Journal of Impact Engineering*, 112, (February 2018), 15–29. ISSN: 0734743X. DOI: <https://doi.org/10.1016/j.ijimpeng.2017.10.007> (cited on pages 2, 3, 6, 7).
- [18] I. Mohagheghian, M. N. Charalambides, Y. Wang, L. Jiang, X. Zhang, Y. Yan, A. J. Kinloch, and J. P. Dear. 2018. Effect of the polymer interlayer on the high-velocity soft impact response of laminated glass plates. *International Journal of Impact Engineering*, 120, (October 2018), 150–170. ISSN: 0734743X. DOI: <https://doi.org/10.1016/j.ijimpeng.2018.06.002> (cited on pages 2, 8).
- [19] X. e. Wang, J. Yang, Q. Liu, and C. Zhao. 2018. Experimental investigations into SGP laminated glass under low velocity impact. *International Journal of Impact Engineering*, 122, (December 2018), 91–108. ISSN: 0734743X. DOI: <https://doi.org/10.1016/j.ijimpeng.2018.06.010> (cited on pages 2, 3, 8).
- [20] J. K. Kuntsche. 2015. *Mechanical behaviour of laminated glass under time-dependent and explosion loading*. German. Springer-Verlag Berlin Heidelberg, Darmstadt, 265. ISBN: 978-3-662-48830-0. DOI: <https://doi.org/10.1007/978-3-662-48831-7> (cited on pages 2, 7).
- [21] M. H. Ghadiri Rad, F. Shahabian, and S. M. Hosseini. 2015. A meshless local Petrov–Galerkin method for nonlinear dynamic analyses of hyper-elastic FG thick hollow cylinder with Rayleigh damping. *Acta Mechanica*, 226, 5, (May 2015), 1497–1513. ISSN: 0001-5970. DOI: <https://doi.org/10.1007/s00707-014-1266-2>. <http://link.springer.com/10.1007/s00707-014-1266-2> (cited on pages 2, 3).
- [22] N. H. Kim. 2015. *Introduction to nonlinear finite element analysis*. (1st edition). Springer, New York, NY, XIV, 430. ISBN: 9781441917461. DOI: <https://doi.org/10.1007/978-1-4419-1746-1>. <https://www.springer.com/gp/book/9781441917454> (cited on page 2).
- [23] Y. T. Gu, Q. X. Wang, and K. Y. Lam. 2007. A meshless local Kriging method for large deformation analyses. *Computer Methods in Applied Mechanics and Engineering*, 196, 9-12, 1673–1684. ISSN: 00457825. DOI: <https://doi.org/10.1016/j.cma.2006.09.017> (cited on pages 2, 3).
- [24] Abaqus. 2013. Abaqus Analysis User’s Guide. (2013). <http://ivt-abaqusdoc.ivt.ntnu.no:2080/v6.14/books/usb/default.htm> (cited on pages 3, 7).
- [25] N. Kumar and V. V. Rao. 2016. Hyperelastic Mooney-Rivlin Model : Determination and Physical Interpretation of Material Constants. *MIT International Journal of Mechanical Engineering*, 6, 1, 43–46. ISSN: 2230-7680. https://www.mitpublications.org/yellow_images/75618-me-book.43-46.pdf (cited on page 3).
- [26] A. Munjiza, D. R. Owen, and N. Bicanic. 1995. A combined finite-discrete element method in transient dynamics of fracturing solids. *Engineering Computations*, 12, 2, (February 1995), 145–174. ISSN: 02644401. DOI: <https://doi.org/10.1108/02644409510799532> (cited on page 3).

- [27] A. Munjiza, E. E. Knight, and E. Rougier. 2012. *Computational mechanics of discontinua. Wiley series in computational mechanics*. Wiley, Chichester, West Sussex, U.K. DOI: <https://doi.org/10.1002/9781119971160> (cited on page 3).
- [28] A. Munjiza, Z. Lei, V. Divic, and B. Peros. 2013. Fracture and fragmentation of thin shells using the combined finite-discrete element method. *International Journal for Numerical Methods in Engineering*, 95, 6, 478–498. ISSN: 1097-0207. DOI: <https://doi.org/10.1002/nme.4511>. <https://doi.org/10.1002/nme.4511> (cited on pages 3, 4).
- [29] L. Guo, J. Xiang, J. P. Latham, and B. Izzuddin. 2016. A numerical investigation of mesh sensitivity for a new three-dimensional fracture model within the combined finite-discrete element method. *Engineering Fracture Mechanics*, 151, (January 2016), 70–91. ISSN: 00137944. DOI: <https://doi.org/10.1016/j.engfracmech.2015.11.006> (cited on page 3).
- [30] W. Gao and M. Zang. 2014. The simulation of laminated glass beam impact problem by developing fracture model of spherical DEM. *Engineering Analysis with Boundary Elements*, 42, 2–7. ISSN: 09557997. DOI: <https://doi.org/10.1016/jenganabound.2013.11.011> (cited on pages 3, 7).
- [31] J. Xiang, A. Munjiza, and J. P. Latham. 2009. Finite strain, finite rotation quadratic tetrahedral element for the combined finite-discrete element method. *International Journal for Numerical Methods in Engineering*, 79, 8, (August 2009), 946–978. ISSN: 00295981. DOI: <https://doi.org/10.1002/nme.2599> (cited on page 3).
- [32] S. Chen, M. Zang, and W. Xu. 2015. A three-dimensional computational framework for impact fracture analysis of automotive laminated glass. *Computer Methods in Applied Mechanics and Engineering*, 294, (September 2015), 72–99. ISSN: 00457825. DOI: <https://doi.org/10.1016/j.cma.2015.06.005>. <https://www.sciencedirect.com/science/article/pii/S0045782515001978> (cited on pages 4, 7, 8).
- [33] GID. 2011. GID, The universal, adaptive and user friendly pre and post processing system for computer analysis in science and engineering. Reference Manual. (2011). http://www.compassis.com/downloads/Manuals/GiD_User_Manual.pdf (cited on page 5).
- [34] J. Xu, Y. Li, X. Chen, Y. Yan, D. Ge, M. Zhu, and B. Liu. 2010. Numerical study of PVB laminated windshield cracking upon human head impact. *Computers, Materials and Continua*, 18, 2, 183–211. ISSN: 1546-2218. DOI: <https://doi.org/10.3970/cmc.2010.018.183>. (cited on page 7).
- [35] A. Vedrtnam and S. J. Pawar. 2017. Laminated plate theories and fracture of laminated glass plate - A review. *Engineering Fracture Mechanics*, 186, 316–330. ISSN: 00137944. DOI: <https://doi.org/10.1016/j.engfracmech.2017.10.020> (cited on page 7).
- [36] M. A. Samieian, D. Cormie, D. Smith, W. Wholey, B. R. Blackman, P. A. Hooper, and J. P. Dear. 2017. Delamination in Blast Resistant Laminated Glass. *21st International Conference on Composite Materials Xi'an, 20-25th August 2017*, August, 20–25. DOI: <https://doi.org/10.1016/j.ijimpeng.2017.09.001> (cited on page 7).
- [37] J. Stampfl and O. Koldenik. 2000. The separation of the fracture energy in metamaterials. *International Journal of Fracture*, 101, 321–345. DOI: <https://doi.org/10.1023/A:1007500325074> (cited on page 7).
- [38] M. Zang and S. Chen. 2012. Laminated glass. In (Second Edition). L. Nicolais and A. Borzacchiello, editors. John Wiley & Guangzhou. DOI: <https://doi.org/10.1002/9781118097298.weoc121> (cited on page 7).
- [39] M. Sahin, C. S. Çetinarslan, and H. E. Akata. 2007. Effect of surface roughness on friction coefficients during upsetting processes for different materials. *Materials and Design*, 28, 2, 633–640. ISSN: 18734197. DOI: <https://doi.org/10.1016/j.matdes.2006.08.005>

- [org/10.1016/j.matdes.2005.07.019](https://doi.org/10.1016/j.matdes.2005.07.019) (cited on page 7).
- [40] M. Fahlbusch. 2007. Zur Ermittlung der Resttragfähigkeit von Verbundsicherheitsglas am Beispiel eines Glasbogens mit Zugstab. German, (March 2007), 1–123. <http://elib.tu-darmstadt.de/diss/000962> (cited on page 7).
 - [41] A. Farsi and J. Xiang. 2019. DEM Plus Manual. (2019) (cited on page 6).
 - [42] J. Zucker, J. Brades, A. New, and A. Toon. 2016. Jabisupra Company Website. (2016). <https://www.jabisupra.co.uk/> (cited on page 6).
 - [43] I. Mohagheghian, Y. Wang, J. Zhou, L. Yu, X. Guo, Y. Yan, M. N. Charalambides, and J. P. Dear. 2017. Deformation and damage mechanisms of laminated glass windows subjected to high velocity soft impact. *International Journal of Solids and Structures*, 109, (March 2017), 46–62. ISSN: 00207683. DOI: <https://doi.org/10.1016/j.ijsolstr.2017.01.006> (cited on page 8).
 - [44] P. Grant, W. Cantwell, H. McKenzie, and P. Corkhill. 1998. The Damage Threshold Of Laminated Glass Structures. *International Journal of Impact Engineering*, 21, 9, (October 1998), 737–746. ISSN: 0734743X. DOI: [https://doi.org/10.1016/s0734-743x\(98\)00027-x](https://doi.org/10.1016/s0734-743x(98)00027-x) (cited on page 8).
 - [45] K. A. D. L. P. Karunarathna. 2013. Low-Velocity Impact Analysis Of Monolithic And Laminated Glass Using Finite Element Method (FEM). March. <https://theses.bham.ac.uk/id/eprint/5067/2/Kuruvita14MPhil.pdf> (cited on page 8).
 - [46] U. A. Dar, W. Zhang, and Y. Xu. 2013. FE Analysis of Dynamic Response of Aircraft Windshield against Bird Impact. *International Journal of Aerospace Engineering*, 2013, (May 2013), 1–12. ISSN: 1687-5966. DOI: <https://doi.org/10.1155/2013/171768> (cited on page 8).
 - [47] X. Zhang, I. K. Mohammed, M. Zheng, N. Wu, I. Mohagheghian, G. Zhang, Y. Yan, and J. P. Dear. 2019. Temperature effects on the low velocity impact response of laminated glass with different types of interlayer materials. *International Journal of Impact Engineering*, 124, (February 2019), 9–22. ISSN: 0734743X. DOI: <https://doi.org/10.1016/j.ijimpeng.2018.09.004> (cited on pages 8, 9).
 - [48] F. Mili. 2012. Effect of the Impact Velocity on the Dynamic Response of E-Glass/Epoxy Laminated Composites. *Arabian Journal for Science and Engineering*, 37, 2, (March 2012), 413–419. ISSN: 13198025. DOI: <https://doi.org/10.1007/s13369-012-0174-9> (cited on page 8).
 - [49] R. A. Behr, P. A. Kremer, L. R. Dharani, F. S. Ji, and N. D. Kaiser. 1999. Dynamic strains in architectural laminated glass subjected to low velocity impacts from small projectiles. *Journal of Materials Science*, 34, 23, (December 1999), 5749–5756. ISSN: 00222461. DOI: <https://doi.org/10.1023/A:1004702100357> (cited on page 8).
 - [50] B. Liu, T. Xu, X. Xu, Y. Wang, Y. Sun, and Y. Li. 2016. Energy absorption mechanism of polyvinyl butyral laminated windshield subjected to head impact: Experiment and numerical simulations. *International Journal of Impact Engineering*, 90, (April 2016), 26–36. ISSN: 0734743X. DOI: <https://doi.org/10.1016/j.ijimpeng.2015.11.010> (cited on page 8).
 - [51] B. H. Kim, K. C. Ahn, and C. W. Lee. 2016. Low Velocity Impact Behaviors of a Laminated Glass. *Smart Science*, 2, 4, (June 2016), 209–213. DOI: <https://doi.org/10.1080/23080477.2014.11665628> (cited on page 8).
 - [52] Kitware. [n. d.] Visualisation Toolkit. (). [vtk.org](http://www.vtk.org) (cited on pages 9–11, 20).
 - [53] H.-P. Bunge. 2009. Earth Models. Munich, (March 2009). <http://www.earthmodels.org> (cited on pages 9–12, 20).
 - [54] J. Aspnes. 2014. C/FloatingPoint. New Haven, Connecticut, (2014). [http://www.cs.yale.edu/homes/aspnes/pinewiki/C\(2f\)FloatingPoint.html](http://www.cs.yale.edu/homes/aspnes/pinewiki/C(2f)FloatingPoint.html) (cited on page 12).
 - [55] D. Apps. [n. d.] Simple online tools. <https://www.pinterest.co.uk/davinapps/simple-online-tools/> (cited on page 13).

- [56] J. Malinen. [n. d.] B64 encoding function. (). <http://web.mit.edu/freebsd/head/contrib/wpa/src/utils/base64.c> (cited on page 13).
- [57] C. Geuzaine and J.-F. Remacle. 2009. Gmsh: a three-dimensional finite element mesh generator with built-in pre- and post-processing facilities. <http://gmsh.info/> (cited on page 19).
- [58] A. Munjiza. 2000. Manual for the “Y” Fem / Dem Computer Program. C, 1–19 (cited on page 25).

Table A1. List of Y2D input simulation parameters [58]

/YD/YDC/MCSTEP	Maximum number of timesteps
/YD/YDC/NCSTEP	Current number of timesteps
/YD/YDC/ISAVE	Restart file saving frequency
/YD/YDC/DCGRAX	Gravity in X Direction
/YD/YDC/DCGRAY	Gravity in Y Direction
/YD/YDC/DCGRAZ	Gravity in Z Direction
/YD/YDC/DCSTEC	Size of timestep
/YD/YDC/DCTIME	Current time
/YD/YDC/DCURELX	Not specified
/YD/YDC/INITER	Not specified
/YD/YDC/ICOUTF	Output frequency
/YD/YDC/ICOUTI	Current number of iterations
/YD/YDC/DCSIZEC	Maximum size of coordinates
/YD/YDC/DCSIZEF	Maximum size of force
/YD/YDC/DCSIZS	Maximum stress
/YD/YDC/DCSIZV	Maximum size of velocity
/YD/YDC/DCSIZD	Maximum size of displacement
/YD/YDC/DCSIZA	Maximum joint aperture
/YD/YDC/DCSTEC	Size of the time step
/YD/YDC/DCTIME	Current time
/YD/YDC/DCRMPT	Load ramping stage
/YD/YDC/DCGRST	Gravity settling stage
/YD/YDC/ICSAVF	Restart save frequency
/YD/YDC/ICOUTP	Number of chars for each number in output
/YD/YDC/ICFMTY	Not specified
/YD/YDC/ICIATY	Not specified